AJP

ISSN : 0971-3093

Vol 29, Nos 10 - 12, October-December, 2020

# ASIAN JOURNAL OF PHYSICS

An International Peer Reviewed Research Journal

Advisory Editors : W. Kiefer & FTS Yu

*Special issue in honor of Prof Francis Yu*

Prof F T S Yu

*Guest Editor : Kehar Singh*

ANITA PUBLICATIONS

FF-43, 1st Floor, Mangal Bazar, Laxmi Nagar, Delhi-110 092, India

B O : 2, Pasha Court, Williamsville, New York-14221-1776, USA ap

**Asian Journal of Physics**

Vol. 29, Nos 10-12 (2020) 773-785

*Available on:* www.asianjournalofphysics.com

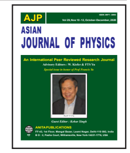

# Off-axis speckle holography for looking through a barrier: A review

Abhijit Roy[1], Rakesh Kumar Singh[2] and Maruthi M Brundavanam[1]

[1]*Department of Physics*, *Indian Institute of Technology Kharagpur, Kharagpur-721 302*, (*W B*), *India*

[2]*Department of Physics, Indian Institute of Technology* (*BHU*), *Varanasi-221 005*, *India*

This article is dedicated to Prof FTS Yu for his significant contributions to Optics and Optical information Processing

This paper presents a review on the application of off-axis speckle holography for looking through an optical barrier. In off-axis speckle holography technique, a titled reference speckle pattern is superposed with an object speckle pattern to retrieve the phase information of the Fourier spectrum of the object embedded into the speckles. The two-point intensity correlation technique along with the phase retrieved utilizing this simple experimental approach, are used to recover the amplitude, phase and polarization information of an object obscured by an optical scattering medium, employing the van Cittert-Zernike theorem. In this review article, theoretical details of the technique along with the experimental results on the optimization of this approach for different 2D imaging, such as, the imaging of complex and polarized objects, are presented. It is also shown that the depth resolved imaging of a 3D object can be achieved exploiting the off-axis speckle holography technique.

**Keywords**: Speckle, Digital holography, Coherence hologram, Coherence and higher order correlations.

## 1 Introduction

The wavefront of a coherent beam of light gets randomized, while passing through a random scattering medium. The temporal coherency of the beam, which remains unaffected by the scattering, enables the scattered light components to interfere among themselves, resulting in a random intensity distribution, known as speckle pattern [1]. The observation of the presence of speckles in a coherent imaging system was reported after the invention of coherent source in 1960s [2,3]. A lot of interest have been generated because of the random intensity distribution of the speckles, and different statistical approaches have been adapted to characterize the speckle pattern in detail [1,4]. However, as the presence of speckles reduces the resolution of coherent imaging systems, various techniques have been developed to reduce the speckles from a system under investigation or to reduce the effect of the scattering [5,6]. Different techniques based on non-linear optics, superposition of large number of uncorrelated speckle patterns, introduction of a rotating diffuser, and temporal averaging of the recorded images have been developed to remove the speckles present in an imaging system [7-10].

The retrieval of an object information based on the holographic approach and using a pre-recorded interferogram established that despite having a random intensity distribution, the speckles contain information about the input beam [11]. A technique based on the holographic approach and using a source of reduced spatial or temporal coherence has been developed to image through a scattering medium [12]. Separately, it has been shown that instead of using a source with short temporal coherence, a source with reduced spatial coherence can be utilized for imaging of objects embedded within a scattering medium [13]. Imaging of a luminous object located inside a scatterer is possible, if the illuminating light is filtered out and the luminescent light from the object is selected for the imaging purpose [14]. Another approach based on the

*Corresponding author :*

*e-mail: bmmanoj@phy.iitgp.ac.in* (Maruthi M Brundavanam)

utilization of the low-coherence gating and spatiotemporal digital holography has been proposed for imaging of object obscured by a scattering medium [15].

The optical phase conjugation, where the phase induced in a beam by a scattering medium is compensated, is another widely used approach for looking through a barrier [16]. The utilization of a spatial light modulator (SLM) or a deformable micro-mirror device to modulate the wavefront of a beam and achieve a desired spatial phase distribution on a beam is extended to the case of scattered light as well for digital nullification of the scatterer induced random phase distribution [17]. Another similar approach, where the wavefront of a beam incident on a scatterer is manipulated using an SLM, is employed for focusing of the input beam inside a strong scattering medium [18]. Recently, an optimization technique along with the wavefront shaping has been used to focus a broad-band light beam in a scattering layer [19]. It has been shown that from proper modulation of the wavefront of an input beam, the polarization information retrieval through a depolarizing medium can be achieved [20]. The difficulty in imaging through a multimode fibre can be addressed employing the wavefront shaping based approach [21]. The penetration depth of the optical coherence tomography in deep tissues, which is used widely for a range of biomedical imaging, has been reported to be increased by incorporating the wavefront shaping based approach [22].

The memory effect based approach for looking through a random scattering medium has been a widely preferred technique during the last decade. The theoretical prediction and the two-point intensity correlation based experimental demonstration of the existence of memory effect of the speckles, which implies that any change in the input beam alters the speckle pattern accordingly, have revolutionized the way of exploiting the speckles for various applications [23, 24]. As the phase information of a speckle pattern is lost in a recorded pattern, the two-point intensity correlation based approach for imaging application requires retrieval of the lost phase of the Fourier spectrum. A technique utilizing the angular memory effect of the speckles along with an iterative based phase retrieval algorithm has been developed for imaging through a scattering medium [25]. The technique proposed in Ref [25] has been simplified for real-life applications by replacing the angular intensity correlation with the two-point intensity correlation of a single speckle pattern [26,27]. The second-order intensity correlation based approach along with a phase retrieval algorithm has been successfully demonstrated for imaging through a fibre bundle, which has tremendous potential applications in the improvement of endoscopic imaging [28]. The imaging and tracking of a moving object, sandwiched between two highly scattering mediums has also been demonstrated using the intensity-correlation-based approach [29].

The intensity-correlation-based approach requires retrieval of the phase information, which is lost in a recorded speckle pattern. Apart from the iteration based phase-retrieval algorithm, different other techniques have also been developed. It has been reported that higher-order intensity correlation of a speckle pattern can be utilized to retrieve the phase information [30]. Recently, another technique based on the bispectrum analysis of a speckle pattern has been demonstrated for the phase-retrieval operation, and has been successfully utilized for imaging through a scattering layer [31]. These proposed techniques for the retrieval of the phase information of a speckle pattern are computationally expensive.

In the holography-based approach, an unknown object beam is interfered with a reference beam, and from the recorded interferogram, using the prior knowledge of the reference beam, the information about the object's spectrum is determined, and this approach can be extended to retrieve the phase information of the object speckles. This method can reduce the complexity of retrieving the phase information, which otherwise requires computation-based approach, which is a complex operation and also faces challenges of convergence and stagnation. In the off-axis speckle holography technique, an object speckle pattern is superposed with a reference speckle pattern of a known correlation feature in the off-axis configuration, and from the recorded speckle interferogram, the lost phase as well as the object information are retrieved. Here, the idea is to overcome the phase recovery challenge in the Hanbury Brown-Twiss (HBT) type approach [32, 33], by combining the off-axis holography with the two point intensity correlation. An analogy between the optical field and complex coherence function has played a very vital role in the development of this method. The off-axis speckle holography technique has been successfully implemented in different types of 2D imaging, such as,imaging of amplitude object, complex object, and polarized object etc. through a scattering layer [33-38]. In a series of papers, we have reported several new developments on combining the correlation features of the random fields with holography, and have presented several new results [33-38]. Some of these techniques are capable of depth-resolved imaging behind a random scattering medium [39]. In this review, the theoretical background of the proposed approach particularly the off-axis holography with coherent waves, and the optimization of the technique along with its experimental demonstration in different imaging applications are discussed in detail.

## 2 Theoretical Details

Let us consider that a monochromatic, spatially random object field vector, $E_{\mathrm{O}}(\mathbf{r}, \mathrm{t})$ can be written in terms of the constituent electric field components $E_{\mathrm{Ox}}(\mathbf{r}, \mathrm{t})$ and $E_{\mathrm{Oy}}(\mathbf{r}, \mathrm{t})$

$$E_{\mathrm{O}}(\mathbf{r},\mathrm{t}) = E_{\mathrm{Ox}}(\mathbf{r},\mathrm{t})\hat{x} + E_{\mathrm{Oy}}(\mathbf{r},\mathrm{t})\hat{y} \tag{1}$$

where $\mathbf{r}$ is the spatial position vector on the transverse observation plane, $t$ is the time, and $\hat{x}$ and $\hat{y}$ are two mutually orthonormal vectors. Techniques based on the determination of the two-point intensity-correlation function of a recorded random intensity distribution or the coherence-polarization (CP) matrix of a random field are exploited for the characterization of a random field distribution. The spatial degree of coherence, $\gamma(\mathbf{r_1}, \mathbf{r_2})$ of a random field can be estimated from the intensity correlation function or the CP matrix, $\Gamma^{\mathrm{O}}(\mathbf{r_1},\mathbf{r_2})$ of the random field. The CP matrix of the object random field can be written as

$$\Gamma^{\mathrm{O}}(\mathbf{r}_1,\mathbf{r}_2) = \begin{bmatrix} \Gamma^{\mathrm{O}}_{\mathrm{xx}}(\mathbf{r}_1,\mathbf{r}_2) & \Gamma^{\mathrm{O}}_{\mathrm{yx}}(\mathbf{r}_1,\mathbf{r}_2) \\ \Gamma^{\mathrm{O}}_{\mathrm{yx}}(\mathbf{r}_1,\mathbf{r}_2) & \Gamma^{\mathrm{O}}_{\mathrm{yy}}(\mathbf{r}_1,\mathbf{r}_2) \end{bmatrix} \tag{2}$$

where the matrix elements are given by $\Gamma^{\mathrm{O}}_{\mathrm{ij}}(\mathbf{r}_1,\mathbf{r}_2) = \langle E^{\mathrm{O}*}_{\mathrm{i}}(\mathbf{r_1})\, E^{\mathrm{O}}_{\mathrm{j}}(\mathbf{r_2})\rangle$. Here,'⟨ ⟩' denotes the ensemble average of the variable. The average intensities of the two orthogonal polarization components of the random field can be estimated from the diagonal elements of the CP matrix at $\mathbf{r_1} = \mathbf{r_2}$, and the trace of the matrix at $\mathbf{r_1} = \mathbf{r_2}$ can be considered as the total average intensity of the random field. The $\gamma(\mathbf{r_1}, \mathbf{r_2})$ of the random field can be written in terms of the two-point intensity correlation function and $\Gamma^{\mathrm{O}}(\mathbf{r_1}, \mathbf{r_2})$ as

$$\gamma^2(\mathbf{r}_1,\mathbf{r}_2) = \frac{\langle \Delta\mathrm{I}(\mathbf{r}_1)\,\Delta\mathrm{I}(\mathbf{r}_2)\rangle}{\langle \Delta\mathrm{I}(\mathbf{r}_1)\,\Delta\mathrm{I}(\mathbf{r}_2)\rangle}\,\frac{\mathrm{tr}[\Gamma^{\mathrm{O}}(\mathbf{r_1}, \mathbf{r_2})\,\Gamma^{\mathrm{O}\dagger}(\mathbf{r_1}, \mathbf{r_2})]}{|\mathrm{tr}[\Gamma^{\mathrm{O}}(0)]|^2} \tag{3}$$

where $\Delta\mathrm{I}(\mathbf{r}) = \mathrm{I}(\mathbf{r}) - \langle \mathrm{I}(\mathbf{r})\rangle$ is the deviation of intensity from its mean value, 'tr' defines the trace of the matrix. The two-point intensity correlation function of the object random field is calculated by inserting Eq (2) in Eq (3), and is found to be

$$\langle \Delta\mathrm{I}(\mathbf{r_1})\,\Delta\mathrm{I}(\mathbf{r_2})\rangle = |\Gamma^{\mathrm{O}}_{\mathrm{xx}}(\mathbf{r_1}, \mathbf{r_2})|^2 + |\Gamma^{\mathrm{O}}_{\mathrm{xy}}(\mathbf{r_1}, \mathbf{r_2})|^2 + |\Gamma^{\mathrm{O}}_{\mathrm{yx}}(\mathbf{r_1}, \mathbf{r_2})|^2 + |\Gamma^{\mathrm{O}}_{\mathrm{yy}}(\mathbf{r_1}, \mathbf{r_2})|^2 \tag{4}$$

It can be observed from Eq (4) that from the study of the intensity correlation function, only the modulus of the complex coherence function of the object random field can be determined. The recovery of the phase is also necessary to construct the complex coherence function, which is used to retrieve the object information from the random field distribution. In order to address this issue, a linearly polarized reference random field, $E_{\mathbf{R}}(\mathbf{r}, \mathbf{t})$ is superposed with the object random field, $E_{\mathbf{O}}(\mathbf{r}, \mathbf{t})$ and the resultant random field can be written as

$$E(\mathbf{r}, \mathbf{t}) = E_{\mathbf{O}}(\mathbf{r}, \mathbf{t}) + E_{\mathbf{R}}(\mathbf{r}, \mathbf{t}) \tag{5}$$

Similar to Eq (2), the CP matrix of the reference random field, $E_{\mathbf{R}}(\mathbf{r}, \mathbf{t})$ can be written as

$$\Gamma^{R}(\mathbf{r}_1,\mathbf{r}_2) = \begin{bmatrix} \Gamma^{R}_{xx}(\mathbf{r}_1,\mathbf{r}_2) & \Gamma^{R}_{yx}(\mathbf{r}_1,\mathbf{r}_2) \\ \Gamma^{R}_{yx}(\mathbf{r}_1,\mathbf{r}_2) & \Gamma^{R}_{yy}(\mathbf{r}_1,\mathbf{r}_2) \end{bmatrix} \tag{6}$$

The spatial degree of coherence, $\gamma_{Res}(\mathbf{r_1}, \mathbf{r_2})$ of the resultant random field, $\mathbf{E}(\mathbf{r}, \mathbf{t})$ is calculated following the intensity correlation based approach, as described in Eq (3), under the following assumptions: both the random fields follow Gaussian statistics, and as the two random fields are experimentally generated from two statistically independent scattering media, and the random fields are mutually uncorrelated. Under the aforementioned assumptions, the $\gamma_{Res}(\mathbf{r_1}, \mathbf{r_2})$ is found to be

$$\gamma^2_{Res}(\mathbf{r}_1,\mathbf{r}_2) = \frac{\langle \Delta I(\mathbf{r}_1)\, \Delta I(\mathbf{r}_2)\rangle}{\langle \Delta I(\mathbf{r}_1)\, \Delta I(\mathbf{r}_2)\rangle} = \frac{\mathrm{tr}[\Gamma(\mathbf{r_1}, \mathbf{r_2})\, \Gamma^{\dagger}(\mathbf{r_1}, \mathbf{r_2})]}{|\mathrm{tr}[\Gamma^{O}(0)]|^2} \tag{7}$$

where, $\Gamma(\mathbf{r_1}, \mathbf{r_2})$ is given by $\Gamma(\mathbf{r_1}, \mathbf{r_2}) = \Gamma^{O}(\mathbf{r_1}, \mathbf{r_2}) + \Gamma^{R}(\mathbf{r_1}, \mathbf{r_2})$ and can be written as

$$\Gamma(\mathbf{r}_1,\mathbf{r}_2) = \begin{bmatrix} \Gamma^{O}_{xx}(\mathbf{r}_1,\mathbf{r}_2) + \Gamma^{R}_{xx}(\mathbf{r}_1,\mathbf{r}_2) & \Gamma^{O}_{xy}(\mathbf{r}_1,\mathbf{r}_2) + \Gamma^{R}_{xy}(\mathbf{r}_1,\mathbf{r}_2) \\ \Gamma^{O}_{yx}(\mathbf{r}_1,\mathbf{r}_2) + \Gamma^{R}_{yx}(\mathbf{r}_1,\mathbf{r}_2) & \Gamma^{O}_{yy}(\mathbf{r}_1,\mathbf{r}_2) + \Gamma^{R}_{yy}(\mathbf{r}_1,\mathbf{r}_2) \end{bmatrix} \tag{8}$$

The expression of $\gamma^2_{Res}(\mathbf{r_1}, \mathbf{r_2})$ can be expanded as follows after inserting Eq (8) in Eq (7)

$$\gamma^2_{Res}(\mathbf{r_1}, \mathbf{r_2}) = \frac{|\Gamma^{O}_{xx}(\mathbf{r_1},\mathbf{r_2})+\Gamma^{R}_{xx}(\mathbf{r_1},\mathbf{r_2})|^2+|\Gamma^{O}_{xy}(\mathbf{r_1},\mathbf{r_2})+\Gamma^{R}_{xy}(\mathbf{r_1},\mathbf{r_2})|^2+|\Gamma^{O}_{yx}(\mathbf{r_1},\mathbf{r_2})+\Gamma^{R}_{yx}(\mathbf{r_1},\mathbf{r_2})|^2+|\Gamma^{O}_{yy}(\mathbf{r_1},\mathbf{r_2})+\Gamma^{R}_{yy}(\mathbf{r_1},\mathbf{r_2})|^2}{|\Gamma^{O}_{xx}(0) + \Gamma^{R}_{xx}(0) + \Gamma^{O}_{yy}(0) + \Gamma^{O}_{yy}(0)|^2} \tag{9}$$

It can be observed from Eq (9) that apart from the dc components due to both the object and reference random fields, $\gamma^2_{Res}(\mathbf{r_1}, \mathbf{r_2})$ also contains interference of the object and reference random fields. These interference terms are exploited to construct the complex coherence function of the object random field, i.e., $\Gamma^{O}(\mathbf{r_1}, \mathbf{r_2})$, using the prior knowledge of the complex coherence function of the reference random field, i.e., $\Gamma^{R}(\mathbf{r_1}, \mathbf{r_2})$. This complex $\Gamma^{O}(\mathbf{r_1}, \mathbf{r_2})$ is utilized to retrieve the object information through a scattering medium.

## 3 Experimental details

A simplified schematic of the experimental setup for the implementation of the off-axis speckle holography technique is shown in Fig 1. A combination of a spatial filter, SF and a lens of focal length of 100 mm is used to clean and collimate a coherent beam of light originating from a He-Ne laser source of wavelength of 632.8 nm. The collimated beam is then split into two using a non-polarizing beam splitter, BS1, and the beam transmitted through BS1 and reflected from M1 makes the object arm of the Mach-Zehnder (MZ) interferometer. An object is placed in the object arm of the MZ interferometer, and depending on the type of the object under investigation, the configuration of the object arm is modified. The object beam is made to pass through a ground glass (GG) plate, GG1, and the speckles generated from GG1 are referred as the object speckles. On the other hand, the beam reflected from BS1 and M2 constitutes the reference arm of the MZ interferometer, the configuration of which is same, as shown in (Fig 1), irrespective of the object in the object arm of the interferometer. In the reference arm, the collimated beam is focused to an off-axis point on another GGP, GG2 using a microscope objective, MO, and the generated speckles are referred to as the reference speckles. The object and reference speckle patterns are superposed using another non-polarizing beam splitter BS2, and the far-field interferogram is recorded using a CCD camera and employing a Fourier arrangement constructed using a lens, $L_2$ of focal length of 200 mm. In the Fourier arrangement, the GGPs are placed at the front focal plane of the lens, whereas the camera is kept at its rear focal plane. Lensless Fourier transform holography for the coherence waves is also possible and this is discussed in Ref [34]. The tilt angle of the MO is adjusted to provide sufficient amount of carrier frequency to the recorded far-field speckle interferogram. It should be noted that if the distance between the MO and GG2 is changed, the beam size on the GG2 gets altered accordingly, which affects the size of the reference speckle grains, which in turn changes the average number of reference speckles (ANRS) present in the recorded speckle pattern due to the finite dimension of the CCD camera. In this paper, first, we have presented the effect of the change in the ANRS on the visibility of the object, retrieved using the off-axis speckle holography, and subsequently, we have presented the results of different types of imaging through a GG plate employing this technique.

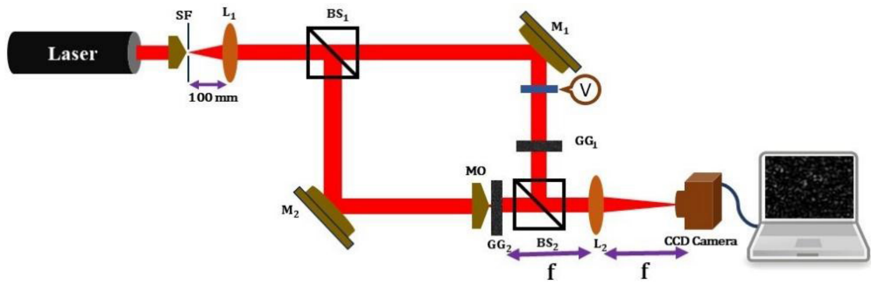


Fig 1. The schematic of the experimental setup for imaging using off-axis speckle holography.

## 4 Result and Discussion

The two-point intensity-correlation technique following Eq (3) is exploited to characterize the far-field speckle patterns recorded for different ANRS. Assuming that the recorded speckle patterns are spatially stationary and ergodic in nature, the ensemble average in Eq (3) is replaced with the spatial average, and the intensity correlation is performed over different spatial points of the recorded speckle pattern. The ANRS present in a recorded speckle pattern is estimated from the ratio of the total area of a recorded speckle pattern and the average effective area covered by a single speckle grain. In order to calculate the average effective area covered by a speckle, the average size of a speckle grain and the average separation between the speckles are required. The full-width at half-maxima (FWHM) of the intensity correlation function of a speckle pattern is considered as the average speckle size. In order to calculate the average separation between the speckles in a speckle pattern, the complement of the speckle pattern is estimated, and the intensity correlation function of the complementary speckle pattern is determined, the FWHM of which is considered as the average separation between the speckles, which has been observed to be same as the average speckle size. The average effective area covered by a single speckle grain is calculated from the average speckle size and the average separation between the speckles, and the ANRS is determined using the calculated average effective area.

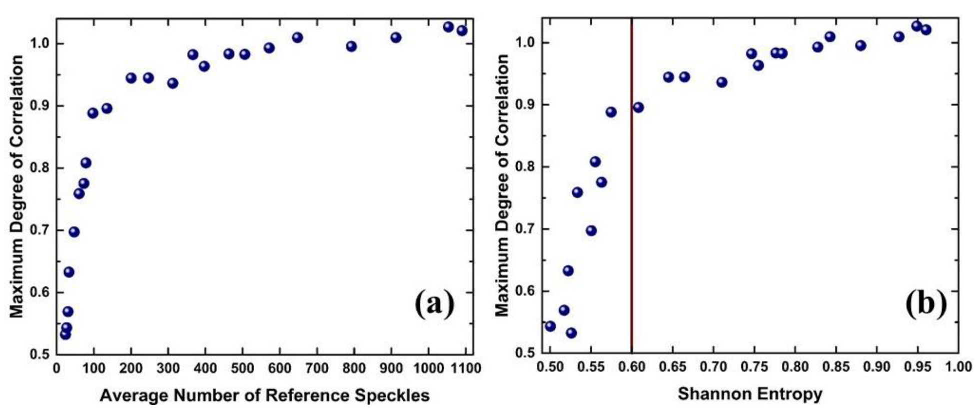


Fig 2. Variation of the maximum degree of correlation of the reference speckle pattern with the (a) ANRS and (b) SE.(Reproduced from Ref 35, with the permission of The Optical Society).

The maximum of the intensity-correlation function of the reference speckle pattern is found to be changing with the ANRS and the variation is presented in Fig 2(a), where it can be observed that although the reference speckle pattern is spatially uniformly polarized, the maximum degree of correlation changes from 0.5 to unity with the increase of the ANRS. This observed variation of the maximum degree of correlation, in case of uniformly polarized speckles, can be explained from the change in the randomness of intensity distribution in the reference speckle pattern with the change of the ANRS. The intensity distribution of the speckle pattern is less random, when the ANRS is less (98 or less), and due to the less randomness, the maximum degree of correlation is observed to be failed to reach the expected value i.e., unity, and in these cases, the maximum degrees of correlation are found to be less than 0.9. On the other hand, when the ANRS is more (135 or more), the intensity distribution of the speckle pattern becomes completely random in nature, and the achieved maximum degrees of correlation in these cases are very close to unity, as expected in case of a spatially uniformly polarized speckle pattern. The change in the randomness of intensity distribution of the speckle pattern with the ANRS is confirmed from the study of the Shannon entropy (SE) of the speckle pattern. It has been found that the SE increases with the ANRS. The variation of the maximum degree of correlation as a function of the SE is also studied and is presented in Fig 2(b), where it can be observed that for SE > 0.6 (ANRS ≥ 135), the maximum degree of correlation is close to unity, which indicates that for SE > 0.6, the intensity distribution of a speckle pattern is completely random in nature. On the other hand, for SE < 0.6 (ANRS ≤ 98), the intensity distribution of a speckle pattern is less random.

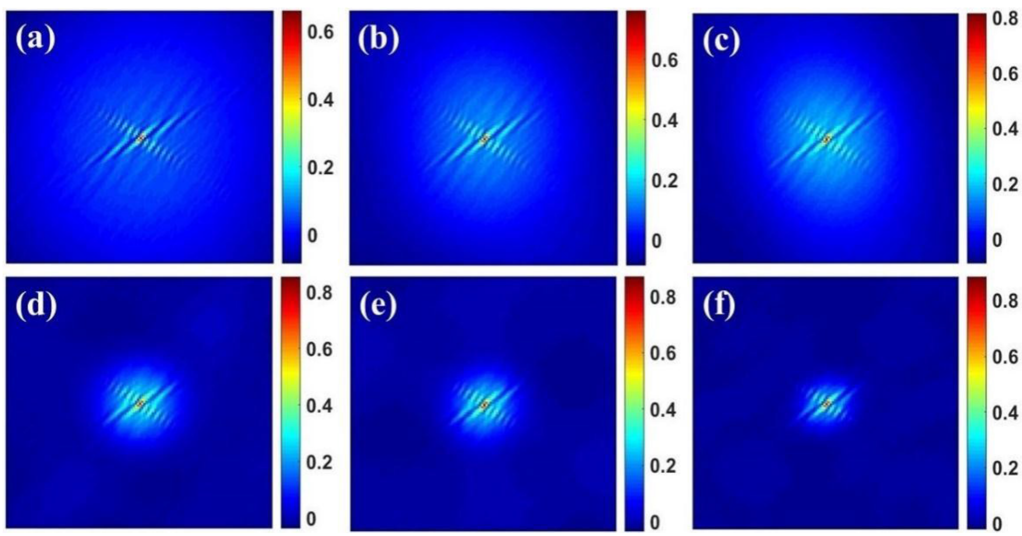


Fig 3. The coherence holograms for ANRS: (a) 31, (b) 74, (c) 98, (d) 397, (e) 572, and (f) 1053. (Reproduced from Ref 35, with the permission of The Optical Society).

The intensity correlation technique, as discussed earlier, is also applied on the recorded far-field speckle interferogram. The intensity-correlation functions of the recorded interferogram for different ANRS are shown in Fig 3, where the presence of fringes can be observed around the centre of the intensity correlation functions. This region around the centre is referred as the coherence hologram (interference of coherent waves). A closer look at the coherence holograms can reveal the presence of a background along with the fringes. The correlation of the interference fringes present in the recorded interferogram leads to the observation of the fringes in the coherence holograms, whereas the correlation of the unmodulated speckles in the interferogram results in the observed background. As the reduction of the speckle size results in the increase of the ANRS, it can be observed that the area of the background to the fringes also reduces with the increase of the ANRS. The coherence holograms presented in Figs 3 (a-c) are in the less random domain, and in Figs 3 (d-f) are in the completely random domain of the reference speckles. It can be found that in the less random domain (Figs 3 (a-c)), with the increase of the ANRS, the number of fringes present in the coherence hologram remains almost invariant. On the other hand, in the completely random domain (Figs 3 (d-f)), the number of fringes is observed to be reducing with the increase in the ANRS. Apart from the maximum degree of correlation of the reference speckle pattern, the change in the ANRS also affects the maximum degree of correlation of the superposed speckle pattern. The colour bars presented along with the intensity correlation functions in Fig 3 show that the square of the maximum degrees of correlation changes from 0.7 to 0.9 with the increase of the ANRS.

Fourier transformation based approach is employed to retrieve the object information from the coherence holograms [40]. The retrieved objects for different ANRS are shown in Fig 4, where apart from the retrieved objects, the presence of dc components at the centre are also observed. The retrieved objects are observed to be present in the second-, and fourth quadrants in Fig 4, and the objects in the fourth quadrants are magnified in the inset. The observed dc component is treated as noise, as its presence reduces the visibility of the retrieved objects. It can be observed that the change of the ANRS affects the visibility of the retrieved object and in the less random domain (Figs 4 (a-c)), the visibility of the retrieved object reduces with the increase in the ANRS. On the other hand, the visibility increases with the ANRS in the completely random domain (Figs 4 (d-f)), although reduction in the sharpness of the retrieved object is also observed.

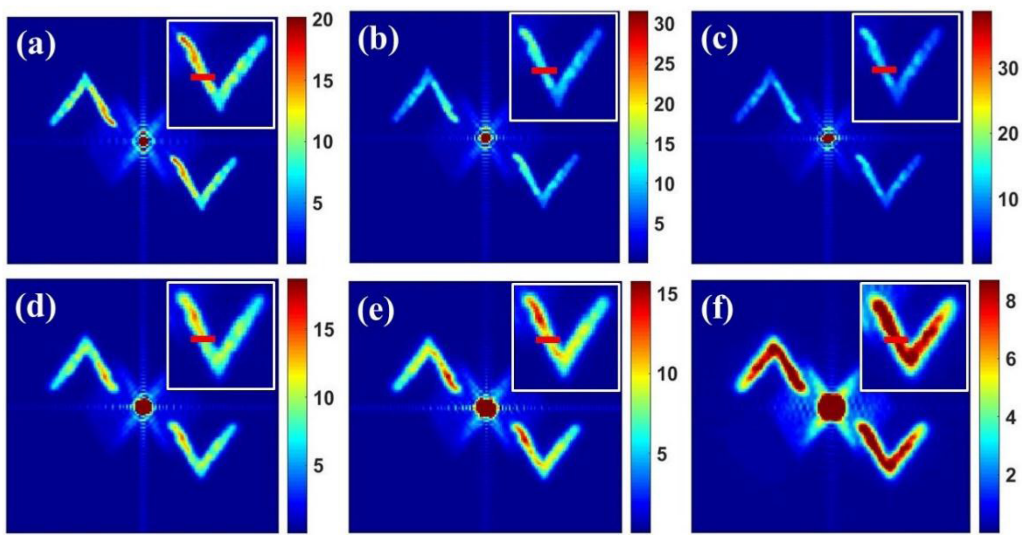


Fig 4. The retrieved objects for ANRS: (a) 31, (b) 74, (c) 98, (d) 397, (e) 572, and (f) 1053. Inset shows the magnified image of the retrieved object. (Reproduced from Ref 35, with the permission of The Optical Society).

In order to study the effect of the change in the ANRS on the visibility of the retrieved objects, the objects present in the second and fourth quadrants in different figures of Fig 4 are normalized with respect to the maximum noise i.e. the maximum of the dc component of the corresponding figure. The visibility of the retrieved object is quantified from the numerical value of the normalized retrieved objects and is referred as the signal-to-noise ratio (SNR). In this study, we focus on the retrieved objects present in the fourth quadrants in Fig 4, which are also magnified in the inset. The maximum SNR of the retrieved objects are observed to be changing with the ANRS, and the variation is presented in Fig 5 (a). It can be observed that initially, the maximum SNR decreases sharply from very close to 1.0 with the increase of the ANRS to reach to a minimum value of 0.4, which corresponds to ANRS = 98. For ANRS ≥ 135,the maximum SNR is found to be increasing slowly with the ANRS and gets saturated at 1.0. This different nature of variation of the maximum SNR with the ANRS in the less random and completely random domain is observed due to the fact that in the less random domain (ANRS ≤ 98), with the increase of the ANRS, the number of unmodulated reference and object speckles increases. This results in a stronger background to the fringes in the coherence holograms leading to lower visibility of the fringes, which causes the observed reduction of the maximum SNR with the increase of the ANRS in the less random domain. On the other hand, in the completely random domain (ANRS ≥ 135), due to the complete randomness of both the object and reference speckles, almost all the object speckles interfere with the reference speckles. This results in the higher visibility of the fringes in the coherence holograms with the increase of the ANRS, leading to the observed higher maximum SNR of the retrieved objects.

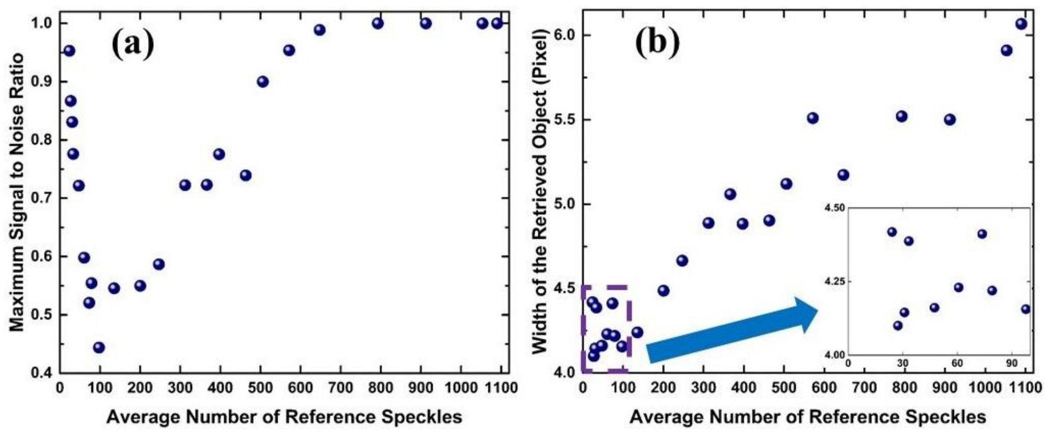


Fig 5. The change of the (a) maximum SNR and (b) width of the retrieved object with the ANRS. (Reproduced from Ref. 35, with the permission of The Optical Society).

Hence, the object information retrieval process can be divided into two domains: less random and completely random distribution of intensity in the reference speckle pattern. In the less random domain, the maximum SNR decreases sharply with the ANRS, whereas in the completely random domain, the maximum SNR increases slowly with the ANRS, although a reduction in the sharpness of the retrieved object is observed. The study of the change in the sharpness with the increase of the ANRS is performed by investigating the change in the width of the retrieved object. In order to determine the width of a retrieved object, a line profile is taken over the retrieved object, and the position of this line profile is kept same for different ANRS, as marked in red for different objects in the inset in Fig 4, and the FWHM of this line profile is considered as the width of the retrieved object.

The variations of the width of the retrieved object as a function of the ANRS is shown in Fig 5 (b). The width is found to be varying randomly without any significant change in the magnitude in the less random domain of the reference speckle patterns i.e. for ANRS ≤ 98, as shown in the inset in Fig 5 (b). However, in the completely random domain i.e. for ANRS ≥ 135, the width is observed to be increasing monotonically with the ANRS. The increase in the width of the retrieved object in the completely random domain of the reference speckles results in the reduction of the sharpness, which is attributed to the decrease in the number of fringes present in the coherent hologram with the increase of the ANRS, as can be observed from Figs 3 (d-f). Hence, high SNR in the retrieved object can be achieved using a less random as well as a completely random reference speckle pattern. However, in case of a completely random reference speckle pattern, the observed reduction in the sharpness of the retrieved object may reduce the resolution of an imaging system, which is not the case in case of the less random reference speckle pattern.

Different types of imaging through a random scattering medium employing the proposed off-axis speckle holography are now presented. It is to be noted that in each different imaging scenario, the object arm of the MZ interferometer in the experimental setup and the data acquisition system are modified, as per the requirement. It has been demonstrated in the earlier paragraphs that using the proposed technique, imaging of 2-D amplitude objects through a random scattering medium can be achieved. In order to demonstrate that a complex object can also be imaged through a random phase plate, the object arm of the setup is modified to encode the complex object. The Gaussian beam in the object arm is split into two, and one of the beam is made to pass through a spiral phase plate, which gives rise to a vortex beam of finite topological charge, the magnitude of which depends on the configuration of the spiral phase plate, at the output of the plate and the generated vortex beam is made to interfere with the unmodulated Gaussian beam. This interference pattern is treated as the object, which is passed through the GG plate in the object arm. The retrieved objects are shown in Figs 6 (a-c), where the fork gratings for vortex beam with topological charge: 3, 6, and 8 are observed. The retrieved fork gratings are Fourier transformed to extract the amplitude and phase profile of the vortex beams, which are shown in the second and fourth quadrants, and in the inset, respectively, in Figs 6 (d-f). This demonstrates the ability of the technique to recover 2D complex objects through a random phase plate.

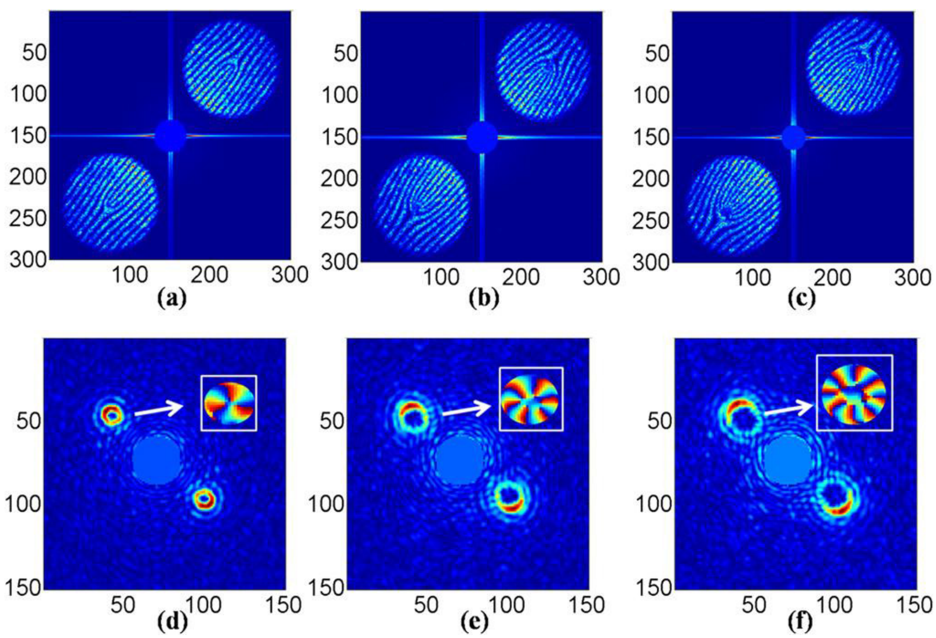


Fig 6. The Fourier transform of the intensity correlation function for input object beam with topological charge: (a) 3, (b) 6, and (c) 8. The retrieved amplitude and the spatial phase profile (in the inset) of the corresponding topological charges.(Reproduced from Ref 36, with the permission of AIP Publishing).

Apart from the retrieval of the amplitude and phase information of an object through a scattering medium, polarization information retrieval is also required to complete the object information retrieval process. Here, it is shown that the off-axis speckle holography can also be exploited for imaging of polarized object. A polarization state generator i.e. a combination of a polarizer and a quarter-wave plate is introduced in the object arm to induce different polarization states, such as linear and elliptical polarizations etc.,to the object beam. In this case, another combination of a quarter-wave plate and a polarizer is placed before the CCD camera. This combination along with the off-axis speckle holography is utilized to construct the complex CP matrix elements of the object random field, which are then Fourier transformed to retrieve the polarization matrix elements of the input object beam at the GG plate. The theoretical prediction along with the experimental result of the polarization matrix elements on the GG plate in case of a linearly polarized object beam are shown in Fig 7. These polarization matrix elements are further utilized to retrieve the polarization information of the input object beam, and the experimental results along with the expected values are presented in Table 1.

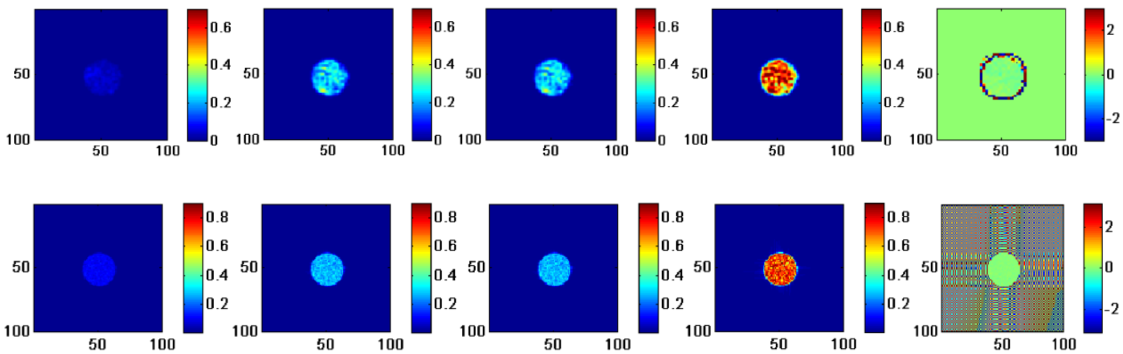

Fig 7. The polarization matrix elements for a linearly polarized object beam on the GG plate from left to right in the following order: xx, xy, yx and yy components, and the phase of the input beam. The first and second row represent the experimental results and the theoretical predictions, respectively. (Reproduced from Ref 37, with the permission of IOP Publishing).

Table 1. The experimental results of the polarization information retrieval (Reproduced from Ref 37, with the permission of IOP Publishing.)

| Parameter | Expected Value | Measured Value |
|---|---|---|
| Ellipticity | 0 | 0.8 |
| | 30 | 29.08 |
| Orientation | 5 | 5.12 |
| | 20 | 20.3 |

Apart from the retrieval of polarization information of an object beam through a non-birefringent scattering medium, it is also possible to image multiple polarized objects through a week birefringent scattering medium using the off-axis speckle holography technique. The beam entering the object arm is split into two mutually orthogonally polarized beams and for the imaging purpose, the beams are made to pass through two letters, here,'H' and 'V' to visually differentiate the two polarization states, and subsequently,these beams are superposed. This superposed beam is referred to as the object beam, and is passed through a weak birefringent scattering medium, which results in a random spatial polarization distribution, commonly referred to as the polarization speckle. It is shown that by modulating the object speckles using a polarizer and employing the off-axis speckle holography, it is possible to retrieve the constituent polarization information of the object beam from the polarization speckle. The experimental results in the absence and presence of the polarizer are presented in Fig 8, where the presence of both the objects in the absence of the polarizer and the retrieval of the constituent polarization components in the presence of the polarizer can be observed.

The imaging of different types of 2D objects through a scattering medium have been demonstrated till this point. We now turn our attention towards the utilization of the off-axis speckle holography in depth-resolved imaging or 3D imaging. The 3D objects, required for this purpose, are introduced in the object arm using a SLM. Fourier holograms for two different sets of letters: 'O' and 'W', and 'star' and 'heart', are generated numerically and are projected on the SLM. In designing the Fourier holograms, in both the sets, the objects are placed in two different quadrants, and the distance between the objects are kept different in the two sets: 10 mm (in case of 'O' and 'W') and 15 mm (in case of 'star' and 'heart'). The GG plate in the object arm is illuminated by theses Fourier holograms displayed on the SLM employing a 4f geometry. The Fourier holograms illuminated on the GG plate are retrieved from the generated speckle pattern exploiting the off-axis speckle holography, and the objects at different depths are reconstructed from the retrieved Fourier holograms, which contain the information of the 3D objects, using a numerical beam propagation technique following the angular spectrum method. The reconstructed amplitude and phase information of the objects at the earlier mentioned depths are shown in Fig 9. The visibility of the reconstructed objects and the reconstruction efficiency are determined both in the presence and absence of the scattering medium, and a good matches are found between these two results. In case of letter 'O', the visibility and the reconstruction efficiency in the absence of the scattering medium are found to be 11.26 and 0.92, respectively, whereas the values in the presence of the scattering medium are 10.70 and 0.91, respectively. This establishes the applicability of the off-axis speckle holography technique in 3D imaging through a random scattering medium.

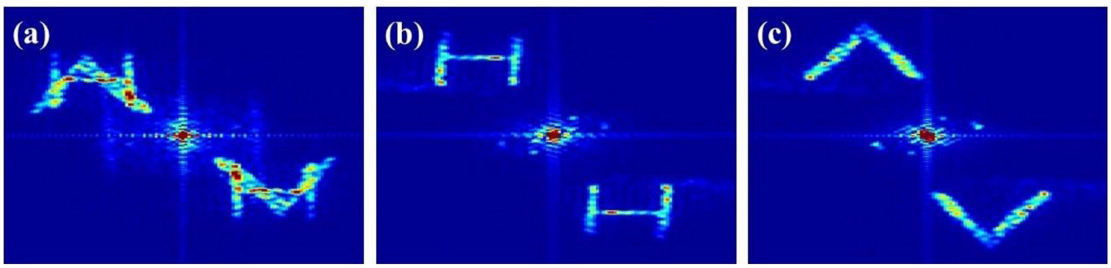


Fig 8. The retrieved polarized amplitude objects (a) without the polarizer and with the polarizer oriented at: (b) 0° and (c) 90°.(Reproduced from Ref 38, with the permission of AIP Publishing).

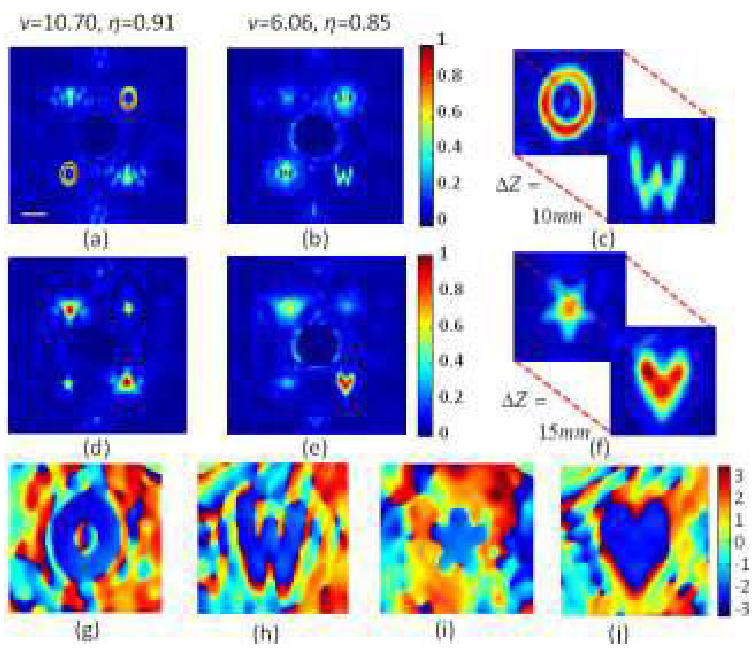


Fig 9. The experimental results of the 3D imaging through a scattering layer. The retrieved amplitude information of the two sets of objects are shown in (a), (b) and (d), (e). The reconstruction of two different objects at two different depths are shown in (c) and (f). The retrieved phase informations are shown in (g)-(i). The values of the visibility and the reconstruction efficiency are shown on the top of the figure (Reproduced from Ref 39, with the permission of The Optical Society).

## 5 Conclusion

In conclusion, in this paper, we have reviewed in detail, the off-axis speckle holography technique and its application in different types of imaging through a random scattering medium in detail. At first, we have investigated the optimization of the technique, where we have observed that the randomness of the intensity distribution in a reference speckle pattern affects the SNR and the sharpness of the retrieved object,and have established that a less-random reference speckle pattern is more suitable for looking through a barrier using this technique. It has been shown that using this technique the amplitude and phase information of 2D amplitude and complex objects can be retrieved. Furthermore, the recovery of the polarization information of 2D objects obscured by a scattering layer is established, which completes the full information retrieval of a 2D object. We have also shown that the depth resolved imaging or 3D imaging at different depths can be achieved using the speckle holography based approach, which further establishes the potentiality of this technique in wide range of imaging applications through a scattering medium.

## Acknowledgements

The authors acknowledge the contributions of other group members from our labs.

## References

1. Goodman J W, Statistical Optics, (Wiley N Y), 2015.
2. Rigden J D, Gordon E I, Granularity of scattered optical maser light, *Proc IRE*, 50(1962)2367-2368.
3. Oliver B M, Sparkling spots and random diffraction, *Proc IEEE*, 51(1963)220-221.
4. Goodman J W, Some fundamental properties of speckle, *J Opt Soc Am*, 66(1976)1145-1150.
5. Dingel B, Kawata S, Speckle-free image in a laser-diode microscope by using the optical feedback effect, *Opt Lett*, 18(1993)549-551.
6. Von Bally G, Schmidthaus W, Sakowski H, Mette W, Gradient-index optical systems in holographic endoscopy, *Appl Opt*, 23(1984)1725-1729.
7. Helmchen F, Denk W, Deep tissue two-photon microscopy, *Nat Methods*, 2(2005)932-940.
8. Völker A C, Zakharov P, Weber B, Buck F, Scheffold F, Laser speckle imaging with an active noise reduction scheme, *Opt Express*, 13(2005)9782-9787.
9. Stangner T, Zhang H, Dahlberg T, Wiklund K, Andersson M, Step-by-step guide to reduce spatial coherence of laser light using a rotating ground glass diffuser, *Appl Opt*, 56(2017)5427-5435.
10. Mehta D S, Naik D N, Singh R K, Takeda M, Laser speckle reduction by multimode optical fiber bundle with combined temporal, spatial, and angular diversity, *Appl Opt*, 51(2012)1894-1904.
11. Leith E N, Upatnieks J, Holographic imagery through diffusing media, *J Opt Soc Am*, 56(1966)523-523.
12. Leith E N, Chen C, Chen H, Chen Y, Dilworth D, Lopez J, Rudd J, Sun P C, Valdmanis J, Vossler G, Imaging through scattering media with holography, *J Opt Soc Am A*, 9(1992)1148-1153.
13. Leith E N, Chen C, Chen H, Chen Y, Lopez J, Sun P C, Dilworth D, Imaging through scattering media using spatial incoherence techniques, *Opt Lett*, 16(1991)1820-1822.
14. Yoo K M, Zang Z W, Ahmed S A, Alfano RR, Imaging objects hidden in scattering media using a fluorescence-absorption technique, *Opt Lett*, 16(1991)1252-1254.
15. Indebetouw G, Klysubun P, Imaging through scattering media with depth resolution by use of low-coherence gating in spatiotemporal digital holography, *Opt Lett*, 25(2000)212-214.
16. Sun Y, Moharam M G, Real-time image transmission and interferometry through a distorting medium using two phase conjugators, *Appl Opt*, 32(1993)1954-1957.
17. Hillman T R, Yamauchi T, Choi W, Dasari R R, Feld M S, Park Y, Yaqoob Z, Digital optical phase conjugation for delivering two-dimensional images through turbid media, *Sci Rep*, 3(2013)1909; doi.org/10.1038/srep01909.
18. Vellekoop I M, Mosk A P, Focusing coherent light through opaque strongly scattering media, *Opt Lett*, 32(2007)2309-2311.

19. Wan L, Ji W, Singh R K, Chen Z, Pu J, Use of scattering layer as a programmable spectrum filter, *IEEE J Quantum Electron*, 55(2019)1-6.
20. De Aguiar H B, Gigan S, Brasselet S, Polarization recovery through scattering media, *Sci Adv*, 3(2017)e1600743;doi. 10.1126/sciadv.1600743.
21. Amitonova L V, Descloux A, Petschulat J, Frosz M H, Ahmed G, Babic F, Jiang X, Mosk A P, Russell P, Pinkse P W H, High-resolution wavefront shaping with a photonic crystal fiber for multimode fiber imaging, *Opt Lett*, 41(2016)497-500.
22. Yu H, Lee P, Lee K, Jang J, Lim J, Jang W, Jeong Y, Park Y, In vivo deep tissue imaging using wavefront shaping optical coherence tomography, *J Biomed Opt*, 21(2016)101406; doi.org/10.1117/1.JBO.21.10.101406.
23. Feng S, Kane C, Lee P A, Stone A D, Correlations and fluctuations of coherent wave transmission through disordered media, *Phys Rev Lett*, 61(1988)834-837.
24. Freund I, Rosenbluh M, Feng S, Memory effects in propagation of optical waves through disordered media, *Phys Rev Lett*, 61(1988)2328-2331.
25. Bertolotti J, Van Putten E G, Blum C, Lagendijk A, Vos W L, Mosk A P, Non-invasive imaging through opaque scattering layers, *Nature*, 491(2012)232-234.
26. Katz O, Heidmann P, Fink M, Gigan S, Non-invasive single-shot imaging through scattering layers and around corners via speckle correlations, *Nat Photonics*, 8(2014)784-790.
27. Singh R K, Anandraj S M, Das B, Quantitative phase-contrast imaging through a scattering media, *Opt Lett*, 39(2014)5054-5057.
28. Porat A, Andresen E R, Rigneault H, Oron D, Gigan S, Katz O, Widefield lensless imaging through a fiber bundle via speckle correlations, *Opt Express*, 24(2016)16835-16855.
29. Newman J A, Luo Q, Webb K J, Imaging hidden objects with spatial speckle intensity correlations over object position, *Phys Rev Lett*, 116(2016)073902; doi.org/10.1103/PhysRevLett.116.073902.
30. Marathay A S, Hu Y, Shao L, Phase function of spatial coherence from second-, third-, and fourth-order intensity correlations, *Opt Eng*, 33(1994)3265-3271.
31. Wu T, Katz O, Shao X, Gigan S, Single-shot diffraction-limited imaging through scattering layers via bispectrum analysis, *Opt Lett*, 41(2016)5003-5006.
32. Chen L, Singh R K, Chen Z, Pu J, Phase shifting digital holography with the Hanbury Brown-Twiss approach, *Opt Lett*, 45(2020)212-215.
33. Singh R K, Vinu R V, Anandraj S M, Retrieving complex coherence from two-point intensity correlation using holographic principle, *Opt Eng*, 53(2014)104102; doi.org/10.1117/1.OE.53.10.104102.
34. Singh R K, Vyas S, Miyamoto Y, Lensless Fourier transform holography for coherence waves, *J Opt*, 19(2017)115705; doi.org/10.1088/2040-8986/aa8b8f.
35. Roy A, Parvin R, Brundavanam M M, Effect of the average number of reference speckles in speckle imaging using off-axis speckle holography, *Appl Opt*, 58(2019)4538-4545.
36. Singh R K, Vinu R V, Anandraj S M, Recovery of complex valued objects from two-point intensity correlation measurement, *Appl Phys Lett*, 104(2014)111108; doi.org/10.1063/1.4869123.
37. Singh D, Chen Z, Pu J, Singh R K, Recovery of polarimetric parameters from non-imaged laser-speckle, *J Opt*, 20(2018)085605; doi.org/10.1088/2040-8986/aacf2d.
38. Roy A, Singh R K, Brundavanam M M, Analysis of polarization speckle for imaging through random birefringent scatterer, *Appl Phys Lett*, 109(2016)201108; doi.org/10.1063/1.4967881.
39. Somkuwar A S, Das B, Vinu R V, Park Y, Singh R K, Holographic imaging through a scattering layer using speckle interferometry, *J Opt Soc Am A*, 34(2017)1392-1399.
40. Takeda M, Ina H, Kobayashi S, Fourier-transform method of fringe-pattern analysis for computer-based topography and interferometry, *J Opt Soc Am*, 72(1982)156-160.


[*Received*: 07.08.2020; *accepted*: 27.08.2020]